

Homeostatic Matching and Nonlinear Amplification at Identified Central Synapses

Hokto Kazama¹ and Rachel I. Wilson^{1,*}

¹Department of Neurobiology, Harvard Medical School, 220 Longwood Avenue, Boston MA 02115, USA

*Correspondence: rachel_wilson@hms.harvard.edu

DOI 10.1016/j.neuron.2008.02.030

SUMMARY

Here we describe the properties of a synapse in the *Drosophila* antennal lobe and show how they can explain certain sensory computations in this brain region. The synapse between olfactory receptor neurons (ORNs) and projection neurons (PNs) is very strong, reflecting a large number of release sites and high release probability. This is likely one reason why weak ORN odor responses are amplified in PNs. Furthermore, the amplitude of unitary synaptic currents in a PN is matched to the size of its dendritic arbor. This matching may compensate for a lower input resistance of larger dendrites to produce uniform depolarization across PN types. Consistent with this idea, a genetic manipulation that lowers input resistance increases unitary synaptic currents. Finally, strong stimuli produce short-term depression at this synapse. This helps explain why PN odor responses are transient, and why strong ORN odor responses are not amplified as powerfully as weak responses.

INTRODUCTION

Neural circuits in different brain regions implement different computations. Part of this diversity likely reflects the connectivity motifs that predominate in each type of circuit (Milo et al., 2002). Equally important, however, are the distinctive properties of these synaptic connections (Walmsley et al., 1998). In order to understand how diverse computations arise from neural assemblies, it will be important to integrate synaptic and circuit-level approaches. Ideally, we would like to examine both the in vivo tuning of specific neurons and the properties of synapses interconnecting them. In practice, however, this can be difficult to achieve.

Invertebrate model systems present special opportunities for integrating synaptic and circuit approaches to neural function. These circuits can be highly accessible in vivo, and because they contain relatively few neurons, the same cells can often be identified in different animals (Comer and Robertson, 2001). Furthermore, invertebrate genetic model organisms offer powerful tools for labeling and manipulating neurons in vivo. However, central synapses in these organisms have not generally received the type of quantitative and detailed electrophysiological investigation that has been performed at many vertebrate synapses in brain slice preparations.

In this study, we set out to describe the properties of identified central synapses in an invertebrate circuit, and to understand how these distinctive properties shape the computations performed by this circuit. The model circuit we use is the *Drosophila* antennal lobe, a brain region analogous to the vertebrate olfactory bulb. The principal neurons of the antennal lobe are called projection neurons (PNs). Like mitral cells of the olfactory bulb, antennal lobe PNs receive direct excitatory synaptic inputs from olfactory receptor neurons (ORNs). Each type of ORN projects to a discrete glomerulus in the antennal lobe and defines an identifiable type of postsynaptic PN (Bargmann, 2006; Hallem and Carlson, 2004; Wilson and Mainen, 2006). One virtue of this model circuit is that specific types of ORNs and PNs can be genetically labeled and identified for functional characterization.

In vivo, this circuit performs several fundamental computations on olfactory signals (Bhandawat et al., 2007). First, the antennal lobe circuit increases the signal-to-noise ratio of odor-evoked spike trains. Individual PN spike trains are highly reliable across repeated presentations of the same odor. In fact, they are more reliable than individual ORN responses. Second, this circuit performs a nonlinear transformation on odor-evoked ORN signals. Weak ORN responses are powerfully amplified in PNs, but strong ORN responses are not amplified to the same degree. Third, the antennal lobe preferentially transmits information about odor onset. Whereas ORNs show maintained responses to odors, PNs only respond robustly to odor onset. Here we show that the unusual properties of ORN-PN synapses can at least partially explain all these features of circuit activity—high reliability, nonlinear amplification, and emphasis of response onset. Moreover, we show that unitary synaptic potentials are constant across glomeruli, although unitary synaptic currents are larger in large glomeruli. This implies that synaptic currents are matched to the characteristic input resistance of each PN type. Consistent with this idea, we find that decreasing input resistance increases unitary synaptic currents in a PN. Hence, the gain of an ORN-PN synapse is kept constant across different PN types. These results illustrate how the distinctive features of identified synapses enable specific in vivo transformations of sensory information.

RESULTS

Direct and Lateral Excitatory Inputs to PNs

Flies perceive odors through two peripheral sensory structures: the antennae and the maxillary palps. Antennal and palp ORNs

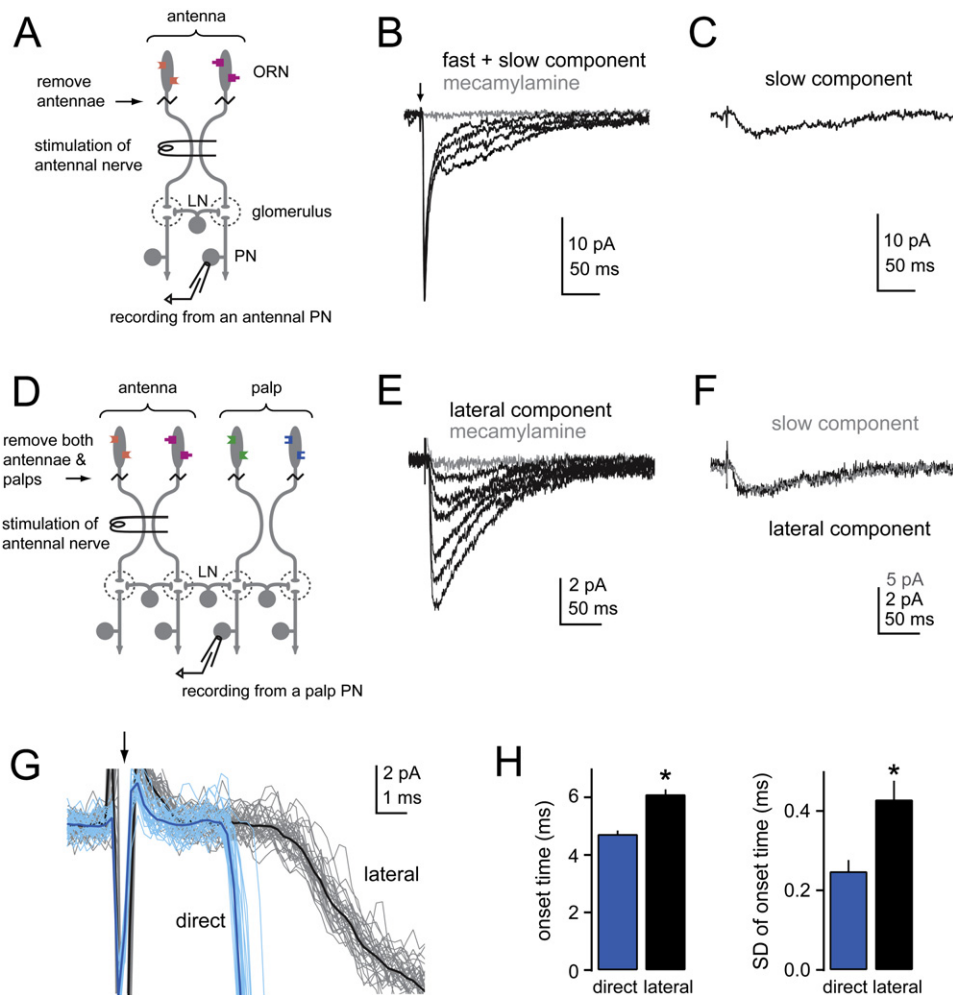


Figure 1. Direct and Lateral Synaptic Inputs to PNs

(A) Schematic of experimental setup. LN, local neuron.

(B) EPSCs recorded in an antennal PN in response to antennal nerve stimulation. A minimal stimulation protocol was employed in order to recruit a single fiber presynaptic to the recorded PN (see Figure 2B and Supplemental Experimental Procedures). Several EPSCs are overlaid to show trial-to-trial variability. Generally, evoked EPSCs had two decay phases. In many experiments, the size of the slow component showed more trial-to-trial variation as compared with the fast component. Mecaminylamine (50 μ M) blocks both components. Arrow indicates stimulus artifact (clipped for clarity).

(C) Occasionally the fast component failed in an all-or-none fashion, revealing the slow component. Trace is an average of six trials, same cell as in (B).

(D) Schematic of experiment designed to isolate lateral inputs to a PN.

(E) Overlay of several EPSCs recorded in a PN postsynaptic to palp ORNs (glomerulus VM7) in response to antennal nerve stimulation. Each trace is an average of ten trials, each at a different stimulus intensity. Only the slow component is present, presumably reflecting lateral excitatory input via cholinergic local interneurons. Mecaminylamine (50 μ M) blocks this response.

(F) The kinetics of the lateral component recorded in a palp PN (black) resemble the kinetics of the slow component recorded in an antennal PN (gray).

(G) Overlay of 34 individual responses to antennal nerve stimulation in an antennal PN (direct component: blue) and a palp PN (lateral component: gray). Average traces are shown in darker colors. Arrow indicates stimulus artifact.

(H) The onset of the lateral component is about 1.5 ms later than the direct component ($p < 10^{-4}$, t test, $n = 32$ direct, 5 lateral), and the jitter of the lateral component is larger than that of the direct component ($p < 0.0005$, t test, $n = 13$ direct, 5 lateral). Onset is the time when a response reaches 10% of its peak.

send their axons to the antennal lobe through the antennal nerve and the maxillary-labellar nerve, respectively (Stocker et al., 1990). In the antennal lobe, ORNs synapse onto nonoverlapping populations of PNs, “antennal PNs” and “palp PNs.” When the antennae and palps are intact, ORNs spike spontaneously and release neurotransmitter onto PNs. This produces a constant barrage of spontaneous excitatory postsynaptic currents (EPSCs). In somatic recordings, spontaneous EPSCs can be

easily distinguished kinetically and pharmacologically from currents produced by unclamped action potentials (Figure S1, available online).

To study the physiology of ORN-PN synapses under more controlled conditions, we acutely removed the antennae, stimulated an antennal nerve with a suction electrode, and monitored responses from antennal PNs using whole-cell patch-clamp recordings (Figure 1A). When we recorded from PNs postsynaptic

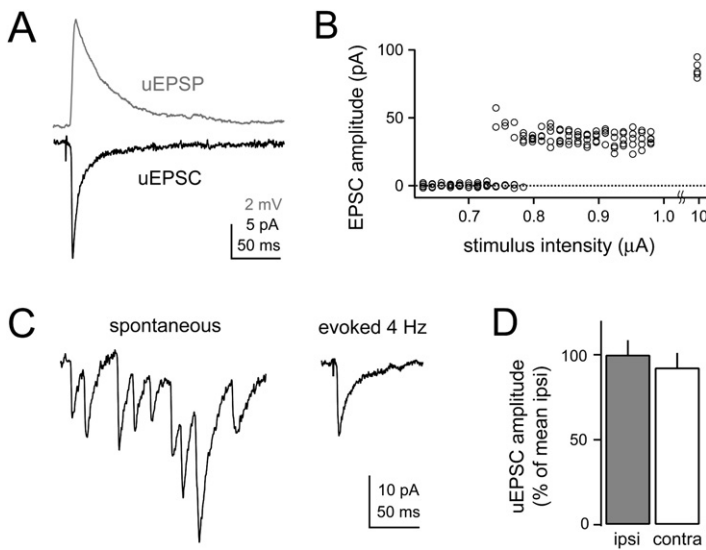


Figure 2. A Single ORN Spike Has a Large and Reliable Impact on a PN

(A) uEPSP (black) and uEPSP (gray) recorded in the same cell (glomerulus VM2). Each trace is an average of three trials.

(B) Minimal stimulation protocol. As stimulus intensity is increased, the fast component of the evoked EPSC appears abruptly. EPSC amplitude then remains constant over a wide range of intensities. This range likely corresponds to stimulation of a single axon presynaptic to this PN. At a much higher stimulus intensity, the amplitude of the evoked EPSC abruptly doubles, presumably reflecting recruitment of a second fiber. The uEPSC amplitude in this experiment is larger than average but within the range observed in the four glomeruli we tested (see Figure 3A and Figure 4A).

(C) Spontaneous EPSCs recorded in a fly with intact antennae and a uEPSC evoked by antennal nerve stimulation mimicking spontaneous ORN firing rates (4 Hz). Both recordings are from PNs in glomerulus DM4.

(D) Ipsilateral and contralateral nerve stimulation evoke uEPSCs of similar size ($p > 0.54$, t test, $n = 20$ ipsilateral, 24 contralateral). PNs are postsynaptic to glomerulus DM6, VM2, DL5, or DM4. Each uEPSC amplitude was normalized to the mean value evoked by ipsilateral stimulation in that glomerulus, and then data for all four glomeruli were pooled.

to antennal ORNs, antennal nerve stimulation evoked an EPSC with a monosynaptic latency (Figure 1B).

The decay phase of these evoked EPSCs typically had two components, fast and slow. These components appeared to be recruited independently. For example, the amplitude of the fast component was generally very consistent (see below and Supplemental Experimental Procedures), but the slow component of the same EPSCs could fluctuate substantially from trial to trial (Figure 1B). Also, nerve stimulation occasionally completely failed to evoke a fast component but still evoked a slow component (Figure 1C). This implies that these two components originate from different synapses. Each PN receives direct excitatory input from several dozen ORNs and indirect excitatory input from many other ORNs via interneurons that interconnect glomeruli (Olsen et al., 2007; Root et al., 2007; Shang et al., 2007). We hypothesized that the fast component of the evoked EPSC represents direct ORN input and that the slow component represents lateral input. To test this idea, we designed an experiment to isolate lateral input to a PN. Instead of recording from PNs postsynaptic to antennal ORNs, we recorded from PNs postsynaptic to palp ORNs while stimulating the antennal nerve (Figure 1D). Because palp ORNs enter the antennal lobes through the maxillary-labellar nerve, PNs postsynaptic to palp ORNs receive no direct input from the antennal nerve. In order to target these PNs selectively, we used an enhancer trap line to label a subset of them with GFP. In palp PNs, electrical stimulation of the antennal nerve evoked smaller and slower EPSCs than those recorded in antennal PNs (Figure 1E). These slow EPSCs must reflect lateral input, probably from interneurons. The response grew gradually when we progressively increased the stimulus intensity (Figure 1E), presumably indicating the recruitment of more ORN input to local interneurons. In amplitude and time course, these responses resembled the slow component of EPSCs recorded in antennal PNs (Figure 1F), implying that the slow portion of dual-component EPSCs (Figure 1B) reflects lateral input to a PN.

The fastest lateral excitatory input to PNs is likely to be disynaptic (rather than trisynaptic). This is because the latency to EPSC onset was only about 1.5 ms longer in palp PNs compared with antennal PNs (Figures 1G and 1H), and this delay is insufficient for multisynaptic propagation (Laurent and Huster, 1988; Pouille and Scanziani, 2001). This result implies that excitatory interneurons receive monosynaptic input from ORNs. As expected, the latency of lateral EPSCs recorded in palp PNs was more variable than the latency of direct EPSCs recorded in antennal PNs (Figures 1G and 1H).

Together, these experiments show that PNs receive both monosynaptic and disynaptic excitation from ORNs. The existence of lateral excitatory input to PNs has previously been inferred from *in vivo* odor responses (Olsen et al., 2007; Root et al., 2007; Shang et al., 2007). Here our results provide further support for the conclusion that interglomerular excitatory connections exist in the antennal lobe. In most of our experiments, the slow component was relatively small, on average only about 1% as large as the fast component at the time when the fast component peaks. Thus, we can isolate a relatively pure monosynaptic input to antennal PNs by measuring amplitudes at the peak of the EPSC evoked by antennal nerve stimulation (see Experimental Procedures). We will exclusively focus on the fast component in this study.

A Single ORN Spike Has a Large and Reliable Impact on a PN

To characterize unitary EPSCs (uEPSCs) evoked by a spike in a single presynaptic axon, we used a minimal stimulation protocol. Beginning from a low intensity that evoked no fast EPSC, we increased the stimulus intensity gradually until a large fast EPSC suddenly appeared in an all-or-none manner (Figures 2A and 2B). Stimulation failures often occurred near this recruitment threshold, but a small increase in intensity stopped failures without changing the amplitude of successes. Further small increases in stimulus intensity generally did not affect the amplitude of the EPSC. At some intensity (generally >120% of the

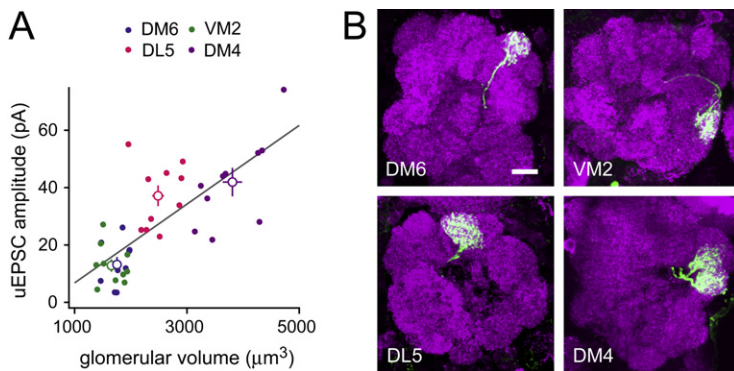


Figure 3. Amplitude of Unitary Synaptic Current Scales with Glomerular Volume

(A) uEPSC amplitude is correlated with the glomerular volume occupied by the PN dendritic tuft (Pearson's $r = 0.75$, $p < 10^{-4}$, $n = 39$). Gray line is a linear fit. Large symbols are mean \pm SEM for each glomerulus.

(B) Each image is a z projection of a confocal stack through a portion of the antennal lobe (neuropil in magenta) showing dendrites of the biocytin-filled PN (green). Some PNs have small dendritic arbors (e.g., glomerulus DM6 and VM2), while others have large dendritic arbors (DL5 and DM4). Scale bar = 10 μ m.

recruitment threshold), EPSC amplitude abruptly increased to roughly double the initial amplitude (Figure 2B). This recruitment profile is evidence that at intensities less than the threshold for the second abrupt increase, we are stimulating a single axon presynaptic to the cell we are recording from (Allen and Stevens, 1994; Stevens and Wang, 1995). If so, the amplitude of the evoked EPSCs should be about the same as the amplitude of spontaneous EPSCs observed in an antennae-intact preparation. To test this prediction, we recorded from PNs in glomerulus DM4 and stimulated the antennal nerve with a minimal stimulus intensity at frequencies approximating the spontaneous firing rates of DM4 ORNs (4 spikes/s; R.I.W., unpublished data). The amplitude of evoked uEPSCs at this stimulus frequency was similar to the amplitude of spontaneous EPSCs we recorded in DM4 PNs with antennae intact (10.7 ± 2.6 pA versus 10.6 ± 1.2 pA, $n = 3$, Figure 2C). Most or all of these spontaneous EPSCs must originate from ORN-PN synapses because they are completely absent when direct ORN input to a glomerulus is removed while lateral inputs are kept intact (data not shown; and see Figure 1 of Olsen et al., 2007). Taken together, all this evidence shows that minimal stimulation can be used in this preparation to study the impact of a single sensory spike on a postsynaptic neuron in the brain.

Across all experiments in several different glomeruli, minimal stimulation of the antennal nerve at 0.033 Hz evoked an average uEPSC measuring 29.0 ± 2.6 pA ($n = 45$) in antennal PNs. These synaptic currents produce very large unitary excitatory postsynaptic potentials (uEPSPs; Figure 2A). Averaged across PNs, uEPSP amplitude was 6.19 ± 0.45 mV ($n = 23$). Thus, a single spike in a single ORN axon has a substantial depolarizing effect on a PN, at least in terms of the membrane potential measured at the soma. This is likely one reason why PNs can respond vigorously to an odor that only weakly excites their presynaptic ORNs. (The convergence of many ORNs onto each PN is another likely reason why weak ORN odor responses are amplified in PNs.)

Most *Drosophila* ORNs project bilaterally to a homologous pair of glomeruli, so we compared EPSCs evoked by stimulating the ipsilateral versus the contralateral antennal nerve. On average, either stimulation site produced an equally large uEPSC (Figure 2D).

Synaptic Current Is Matched to Glomerular Intrinsic Properties

Next, we asked whether synaptic efficacy varies across glomeruli. We measured the average amplitude of evoked uEPSCs in four different types of PNs (postsynaptic to glomerulus DM6,

VM2, DL5, or DM4), and found significant glomerulus-dependent differences within this sample (Figure 3A, $p < 10^{-6}$, ANOVA). Specifically, uEPSC amplitudes are consistently larger for glomeruli DL5 and DM4 than for DM6 and VM2. Thus, the efficacy of ORN-PN synapses is a stereotyped function of glomerular identity.

Interestingly, these four glomeruli have very different sizes. In general, antennal lobe glomeruli vary widely in size, and the size of each glomerulus is stereotyped across individuals (Couto et al., 2005; Fishilevich and Vosshall, 2005; Laissue et al., 1999). Because the dendritic arbor of a PN fills an entire glomerulus, PNs postsynaptic to large glomeruli have characteristically large dendritic arbors. We noticed that the PNs with large uEPSCs (DL5 and DM4) have large dendritic arbors, while PNs with small uEPSCs (DM6 and VM2) have small dendritic arbors (Figure 3B). The correlation between synaptic currents and glomerular volume was strong and highly significant (Figure 3A).

Although unitary synaptic currents differ across glomeruli, uEPSP amplitudes are relatively constant across glomeruli (Figures 4A–4C). Because large dendritic arbors will have a large membrane surface area, they likely have a lower input resistance (see Figure S2). If this were true, then a larger synaptic current would be required to produce the same amount of postsynaptic depolarization in a PN with a large dendritic arbor, as compared with a PN with a small dendritic arbor. This suggests that synaptic currents in these neurons might be homeostatically regulated to produce a fixed level of postsynaptic excitation.

We therefore asked whether there is a causal relationship between postsynaptic input resistance and synaptic current amplitude. In order to lower input resistance, we overexpressed a potassium channel ($Kir2.1^{AAE}$, Paradis et al., 2001) in PNs postsynaptic to glomerulus DM4 or DL5. This produced a significant decrease in the input resistance of these PNs (Figure 4D). Moreover, evoked uEPSC amplitudes were significantly increased in these PNs compared with the same PNs in wild-type flies (Figure 4E). This demonstrates that synaptic strength can be homeostatically adjusted in these cells to compensate for reduced postsynaptic excitability. It should be noted that we are measuring input resistance at the soma, and we do not know how the input resistance of the dendritic compartment contributes to this measurement (see Figure S2). Also, $Kir2.1^{AAE}$ overexpression hyperpolarizes the resting potential in addition to decreasing input resistance (data not shown, see also Paradis et al., 2001), and we do not know which of these effects is

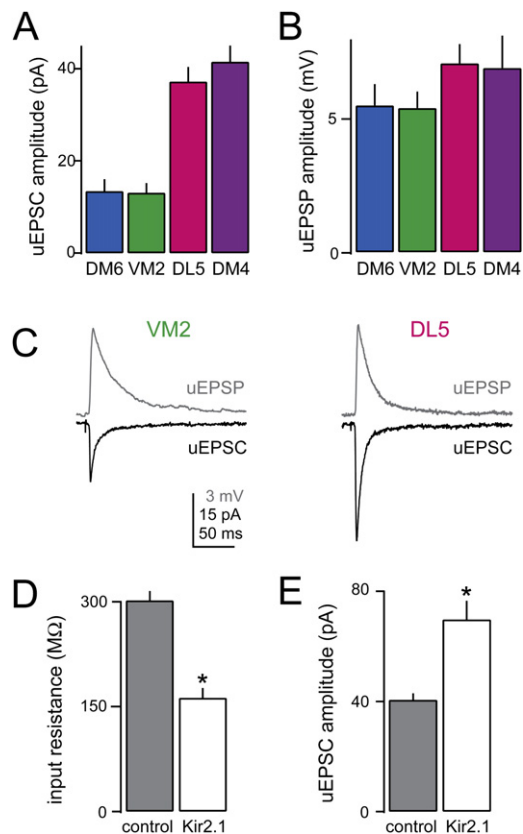


Figure 4. Synaptic Currents Are Matched with Intrinsic Properties of PNs to Produce Constant Postsynaptic Depolarization

(A) uEPSC amplitudes differ across glomeruli ($p < 10^{-6}$, ANOVA, $n = 9, 10, 9$, and 10 for DM6, VM2, DL5, and DM4, respectively).

(B) uEPSP amplitudes are similar across glomeruli ($p > 0.43$, ANOVA, $n = 7, 5, 5$, and 6 for DM6, VM2, DL5, and DM4, respectively).

(C) Representative uEPSC and uEPSP for a PN in glomerulus VM2 versus DL5. EPSPs are similar for both VM2 and DL5, even though EPSCs are larger in DL5. Each trace is an average of several trials.

(D) Overexpression of the Kir2.1^{AAE} potassium channel specifically in a subset of PNs decreases the input resistance recorded at the soma of those PNs ($p < 10^{-6}$, t test, $n = 26$ and 9 for control and Kir2.1^{AAE}, respectively). Genotypes are *NP3062-Gal4,UAS-CD8:GFP* (control) and *NP3062-Gal4,UAS-CD8:GFP/+; UAS-Kir2.1^{AAE}-GFP/+* (Kir2.1^{AAE}). All PNs are postsynaptic to glomerulus DL5 or DM4. Data collected in these two glomeruli are pooled but the result is similar if glomeruli are analyzed separately.

(E) uEPSC amplitudes are larger in PNs expressing Kir2.1^{AAE} compared with those of control PNs ($p < 0.005$, t test, $n = 26$ and 7 for control and Kir2.1^{AAE}, respectively).

responsible for triggering the change in EPSC amplitudes. In either case, our result shows that synaptic currents are scaled to match the intrinsic properties of PNs. This supports the idea that the large uEPSCs in PNs with large dendritic arbors reflect a homeostatic compensation for the intrinsic difficulty of depolarizing these cells.

Each ORN Spike Releases Many Vesicles onto Each PN

To investigate why ORN-PN synapses are so strong, we examined three parameters that determine synaptic strength (Katz, 1969):

- (1) the response of a PN to a vesicle of neurotransmitter (quantal size, q),
- (2) the probability of vesicular release at each presynaptic release site (p), and
- (3) the number of vesicular release sites per ORN axon (N).

All three of these parameters can be estimated using the technique of multiple-probability fluctuation analysis (Clements, 2003; Clements and Silver, 2000; Silver, 2003). This involves measuring uEPSC mean and variance under several different conditions of release probability (Figure 5A). The resulting variance-mean plot (Figure 5B) produces estimates of q , N , and p for each cell (see Supplemental Experimental Procedures).

We performed this analysis for PNs in glomeruli DL5 and DM4, and obtained similar results for these two types of PNs (Figure 5C). In these experiments, the average estimated quantal size was 1.05 pA. Estimated release probability was consistently high, with a mean value of 0.79. The number of release sites was also high, with a mean value of 51. Thus, each ORN spike releases dozens of vesicles onto each postsynaptic PN.

The Number of Presynaptic Release Sites per Axon Scales with Glomerular Size

Why are synaptic currents larger for PNs with large dendritic arbors? To address this question, we compared N , p , and q at ORN-PN synapses in different glomeruli. We were not able to apply multiple-probability fluctuation analysis to all glomeruli because when uEPSC amplitudes are small (in glomeruli DM6 and VM2), reducing p reduces uEPSCs to a level near the limit of the recording noise. We therefore turned to an alternate method that does not involve reducing p . We verified that this method produces values in broad agreement with multiple-probability fluctuation analysis (see below), and used it to compare synaptic parameters of all four glomeruli in our data set.

We can directly measure q from the amplitudes of miniature EPSCs (mEPSCs; recorded in 1 μ M tetrodotoxin; Figure 6). Most of these mEPSCs are likely to arise from ORN-PN synapses, because when we removed ORN axons from a few glomeruli while leaving ORN inputs to other glomeruli intact, the majority of mEPSCs disappeared (Figure S3). A minority of mEPSCs arise from other sources, however, meaning that this analysis should be interpreted with caution (Figure S3). This method produced estimates of q similar to estimates from multiple-probability fluctuation analysis, although slightly larger (see below, and also Meyer et al., 2001). PNs in different glomeruli had similar mEPSC amplitudes (Figure 6C), implying that all these PNs are equally sensitive to a vesicle of acetylcholine. The rise time and decay time of mEPSCs were also similar (Figure 6C).

Given these values of q , we can estimate N and p from measurements of uEPSC mean and variance at a single release probability (Figures 7A and 7B, see Supplemental Experimental Procedures). This analysis produced high estimates of p , in agreement with the results of multiple-probability fluctuation analysis. Estimates of p were uniform across glomeruli (Figure 7C). However, unlike values of q and p , values of N were significantly larger in large glomeruli (Figure 7D). This implies that uEPSCs are larger in these glomeruli because the number of presynaptic release sites per ORN fiber is higher for

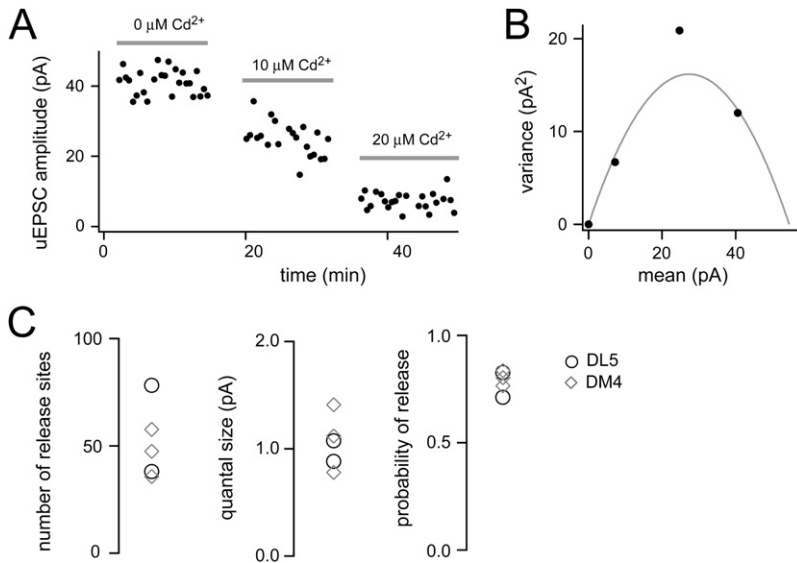


Figure 5. Each Unitary Connection Corresponds to Many Release Sites with a High Probability of Release

(A) A representative multiple-probability fluctuation analysis experiment. Release probability is lowered by adding increasing amounts of Cd^{2+} to the external saline. Epochs during which the mean and the variance of uEPSC amplitudes are calculated are shown for each Cd^{2+} concentration. Recording is from a PN in glomerulus DM4.

(B) Relationship between variance and mean of the uEPSC amplitude for each Cd^{2+} concentration (same cell as in [A]). Parabolic fit yields an estimate of N , q , and p . For this experiment, $N = 47.4$, $q = 1.12$ pA, $p = 0.77$.

(C) Estimated N , q and p for glomerulus DL5 and DM4. Mean values are $N = 51.4 \pm 7.8$, $q = 1.05 \pm 0.11$ pA, and $p = 0.79 \pm 0.02$. We could not apply this method to glomeruli with small uEPSCs (DM6 and VM2) because in Cd^{2+} EPSCs were too small to measure reliably.

these synapses. If differences in synaptic currents across glomeruli reflect a homeostatic matching process, as we have proposed, then this seems to be accomplished by scaling N rather than p .

All our analyses of quantal parameters—both here and in the previous section—assume that release probability is uniform across release sites. We also assume uniformity over time, but in reality we observed a small run-down in uEPSC amplitudes over the course of some long multiple-probability fluctuation analysis experiments. In a multiple-probability fluctuation analysis, a gradual run-down in q will cause an overestimate in N (Figure S4). This may explain why this method produces slightly lower estimates of q and higher estimates of N , as compared

with our second method. Alternatively, this type of discrepancy would also occur if some small mEPSCs fell below the limit of our recording noise, causing an overestimate of q in the second method. Another important assumption of both methods is that responses to single quanta add linearly. This would not be true if, for example, postsynaptic receptors were saturated. We therefore verified that uEPSCs do not saturate receptors at this synapse (Figure S5). We also verified that variability in the size of the slow (lateral) EPSC component has little effect on variance in peak EPSC amplitude (Figure S6). Taken together, these control experiments argue that fluctuations in uEPSC amplitude accurately reflect fluctuations in the number of vesicles released on different stimulus trials.

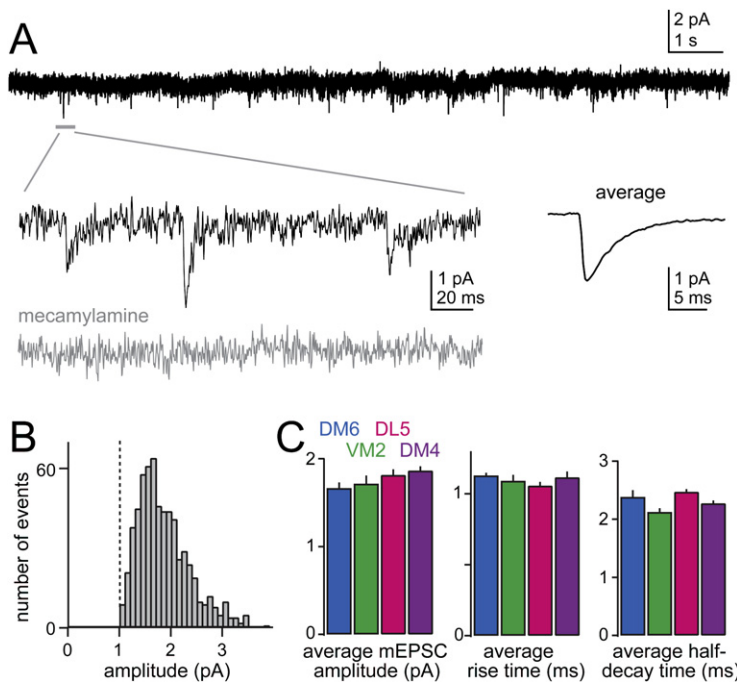


Figure 6. Quantal Events Are Small and Invariant across Glomeruli

(A) Sample trace showing mEPSCs recorded in a VM2 PN, with an enlarged view below. Mecamylamine ($50 \mu\text{M}$) blocks mEPSCs (gray trace). At lower right is an average of 640 mEPSCs recorded in the same cell.

(B) Histogram of mEPSC amplitudes (same cell as in [A]). Dotted vertical line is threshold for mEPSC detection. The CV of mEPSC amplitudes, averaged across all PNs, was 0.24.

(C) Average amplitude, rise time, and half-decay time of mEPSCs recorded in different PN types. There are no significant differences across glomeruli ($p > 0.07$, ANOVA; $n = 7, 4, 6,$ and 5 for DM6, VM2, DL5, and DM4, respectively).

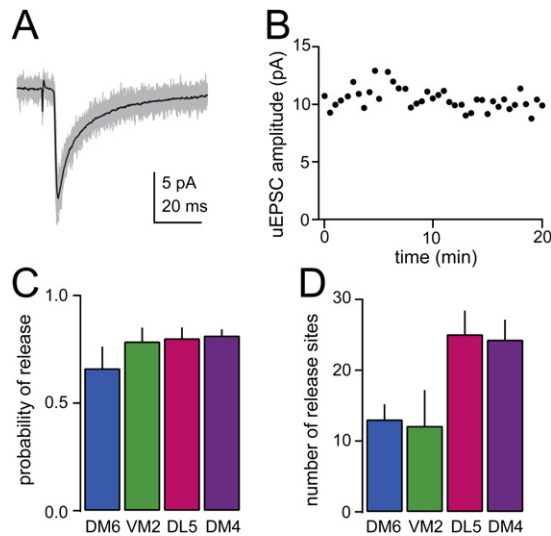


Figure 7. The Number of Release Sites per Axon Scales with Glomerular Size

(A) Overlay of 40 individual evoked uEPSCs (average in black, glomerulus VM2).

(B) Plot of uEPSC amplitude over time showing low variability across trials (same cell as in [A]).

(C) Mean estimated probability of release is high in all PN types (no significant differences across glomeruli, $p > 0.36$, ANOVA, $n = 7, 4, 6,$ and 5 for DM6, VM2, DL5, and DM4, respectively).

(D) Mean estimated number of release sites differs across glomeruli ($p < 0.01$, ANOVA, same cells as in [C]).

Short-Term Depression at ORN-PN Synapses Emphasizes Stimulus Onset

PN responses decline rapidly after odor onset, especially when initial PN firing rates are high. This phenomenon must arise in the antennal lobe, since ORN odor responses generally do not show this rapid decay (Figures 8A and 8B, see also Bhandawat et al., 2007). We therefore asked whether short-term depression at ORN-PN synapses might partly explain this phenomenon. These experiments were also motivated by our observation that ORN-PN synapses show a uniformly high probability of release (Figure 5C and Figure 7C), which should tend to increase short-term depression (Zucker and Regehr, 2002).

First, we examined the possibility that PN responses decline rapidly because of some change in intrinsic PN conductances. Sustained current injection at the soma produces PN firing rates that are quite constant over time (Figure 8C). Thus, a change in PN intrinsic conductances is unlikely to account for the large decline in odor-evoked PN responses over this time interval.

We next asked whether ORN-PN synapses show short-term depression. In these experiments, we stimulated an antennal nerve in patterns that mimic natural ORN spike trains. We recorded from PNs in a glomerulus (VM2) whose presynaptic ORNs have been characterized extensively (Bhandawat et al., 2007; Elmore et al., 2003; Hallem et al., 2004). These ORNs fire spontaneously at about 7 spikes/s (R.I.W., unpublished data). To mimic this, we began every trial with a long train of pulses at this frequency (Figures 8D–8G), which itself produced some synaptic depression. This was immediately followed by a second

train mimicking a variable level of odor-evoked ORN input. All stimulus frequencies produced additional substantial synaptic depression (Figure 8F). As expected, depression was particularly rapid at high stimulus frequencies.

Given the high release probability at ORN-PN synapses, it is likely that presynaptic vesicle depletion contributes to this phenomenon. Consistent with this idea, stimulation at 7 Hz caused a decrease in $1/CV^2$ (CV , coefficient of variation) of uEPSCs, which is linearly correlated with the magnitude of synaptic depression (Figure 8G). Because $1/CV^2$ is linearly correlated with $Np/(1-p)$ for a binomial process, this result indicates a mainly presynaptic origin for synaptic depression at this stimulus frequency (Faber and Korn, 1991). This may, of course, reflect presynaptic inhibition in addition to presynaptic vesicle depletion. At higher stimulus frequencies, postsynaptic factors (such as receptor saturation or desensitization) may also play a role. Whatever the mechanisms, these results demonstrate that ORN spikes have a diminished impact on postsynaptic PNs over time. This, in turn, helps explain why PNs preferentially signal the onset of ORN spike trains.

Short-Term Synaptic Depression Produces a Nonlinear Transformation of ORN Responses

In vivo, an individual ORN responds to multiple odors, with different odors eliciting different average firing rates in that ORN. In general, most odors elicit weak or nonexistent responses in a given ORN. Only a handful of odors elicit strong responses. In other words, most ORNs are somewhat narrowly tuned (Bhandawat et al., 2007; de Bruyne et al., 1999, 2001; Hallem and Carlson, 2006; Hallem et al., 2004). PNs, however, are more broadly tuned to odors (Bhandawat et al., 2007; Wilson et al., 2004). This reflects the fact that weak ORN responses are greatly amplified in postsynaptic PNs, but strong ORN responses are not amplified to the same degree (Figure 9A, reproduced from Bhandawat et al., 2007).

We asked whether short-term depression at ORN-PN synapses could partly explain this nonlinear transformation in odor response profiles. We stimulated ORN axons with a range of frequencies (Figure 9B). As expected, total charge transfer over the duration of a train does not increase in proportion to the stimulus frequency (Figures 9C and 9D). This relationship between charge transfer and presynaptic stimulus frequency (Figures 9C and 9D) is similar to the relationship between odor-evoked PN and ORN firing rates (Figure 9A). Thus, short-term depression at ORN-PN synapses can contribute to the nonlinear amplification of ORN odor responses in PNs.

DISCUSSION

Strong and Reliable Sensory Synapses

Our results show that ORN-PN synapses are strong. Each contact between a single ORN axon and a PN comprises many vesicular release sites. The precise number of sites varies across glomeruli, but our analyses suggest that each axon projecting to a large glomerulus corresponds to >25 release sites per postsynaptic PN. Moreover, the probability of vesicular release from each site is unusually high, near 0.75. Notably, the probability of

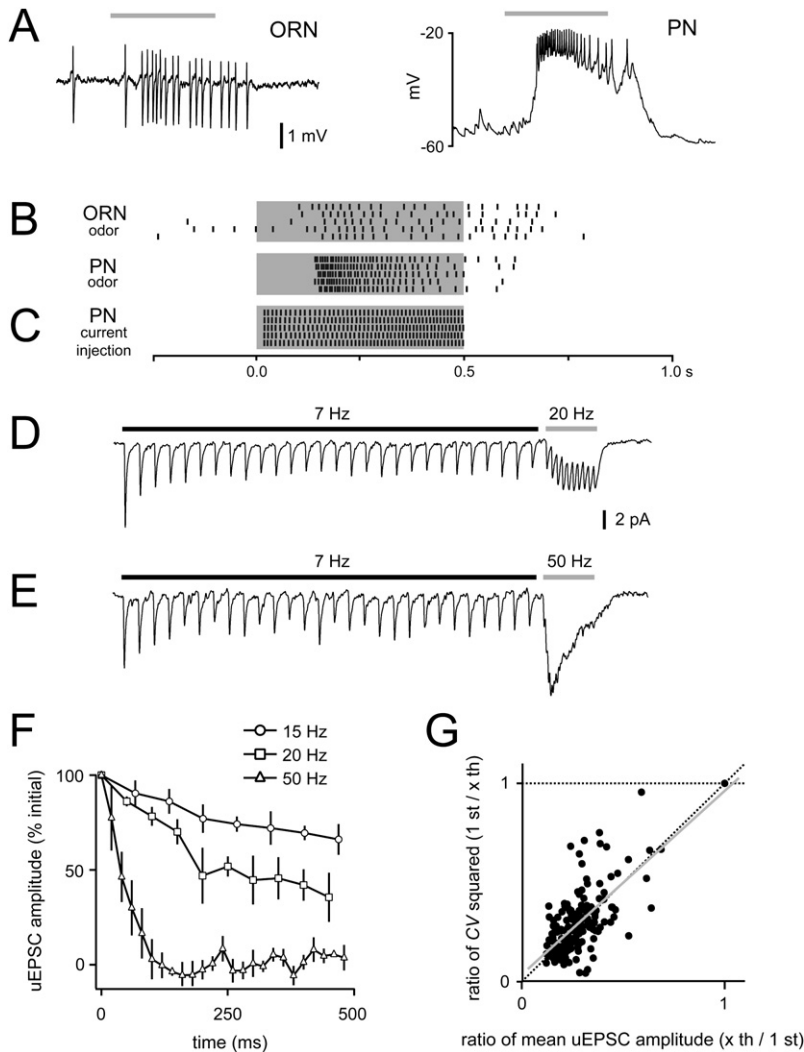


Figure 8. Short-Term Depression at ORN-PN Synapses Emphasizes the Onset of ORN Odor Responses

(A) Raw voltage traces showing typical odor responses in an ORN (left, extracellular recording from a single antennal sensillum) and a PN (right, whole-cell recording). Both are responses to the odor 2-octanone, and both the ORN and the PN correspond to glomerulus DM4. Note the different temporal profile of these responses. Gray bar indicates 500 ms period of odor stimulation. (B) Rasters compare the different temporal profile of these odor-evoked spike trains (same cells and same odor as in [A]). Gray bar indicates 500 ms period of odor stimulation.

(C) Raster plots of spikes evoked by somatic current injection in a PN. Gray bar indicates 500 ms period of current injection. Even when injected current was sufficient to produce firing rates >100 spikes/s, PN responses did not decline over the course of 500 ms (final firing rates were 104.2% of the initial rate, $n = 8$ cells).

(D) uEPSCs evoked by antennal nerve stimulation mimicking spontaneous ORN firing rates (7 Hz, 4 s, black bar) and weak odor-evoked input (20 Hz, 500 ms, gray bar). Traces are averaged over several trials and low-pass filtered to remove stimulus artifacts. All data in (D)–(G) are recordings from PNs in glomerulus VM2. (E) Same as (D), but now mimicking stronger odor-evoked input (50 Hz, 500 ms, gray bar).

(F) Change in uEPSC amplitude during the 500 ms stimulation period mimicking odor-evoked input. Strong inputs rapidly depress ORN-PN synapses ($n = 6$ cells). (G) Repetitive stimulation (7 Hz) causes a decrease in inverse of the square of the coefficient of variation ($1/CV^2$), which is correlated with the decrease in uEPSC amplitude, implying a presynaptic locus for this depression. Gray line is a linear fit (Pearson's $r = 0.79$, $p < 10^{-4}$).

release is also exceptionally high at ORN synapses onto neurons in the vertebrate olfactory bulb (Murphy et al., 2004).

As a result, each ORN spike releases dozens of vesicles of neurotransmitter onto each postsynaptic PN. This contrasts with the situation at many synapses in the mammalian brain, for example excitatory synapses onto hippocampal CA1 pyramidal neurons. At these synapses, each spike rarely releases more than one vesicle onto each postsynaptic cell (Stevens and Wang, 1995), although simultaneous release of a few vesicles can occur at higher firing rates (Christie and Jahr, 2006; Oertner et al., 2002). Indeed, many excitatory synapses in the mammalian brain can release at most one vesicle (Biro et al., 2005; Sargent et al., 2005; Silver et al., 2003).

The strength of ORN-PN synapses has important consequences for the way PNs respond to odors. A comparison of ORN and PN odor responses in vivo demonstrates that PNs are extremely sensitive to weak levels of ORN input (Bhandawat et al., 2007). Odors that evoke small responses in ORNs (<20 spikes/s) can evoke much stronger responses in postsynaptic PNs (>100 spikes/s). This is due in part to the fact that each

PN pools inputs from many converging ORNs. However, the degree of amplification also depends critically on the strength of ORN-PN synapses. Our results show that at low stimulus frequencies (0.033 Hz), a single spike in one ORN axon is sufficient to depolarize a PN by about 6 mV. At frequencies mimicking the basal firing rate of a typical ORN (7 Hz), synaptic responses depress by about 40% but remain relatively strong.

In Diptera, most ORNs synapse bilaterally in both brain hemispheres (Stocker et al., 1990; Strausfeld, 1976), and we have found that ORN-PN synapses are equally strong for both ipsilateral and contralateral ORN projections. This effectively doubles the strength of ORN input as compared with an olfactory system with unilateral ORN projections.

Finally, ORN-PN synapses are highly reliable, with an average CV of just 0.16. This is likely to be part of the explanation for why PN odor responses are so reliable. Indeed, PN responses are more reliable than ORN responses (Bhandawat et al., 2007). This improvement in reliability must stem primarily from the fact that each PN pools direct input from many ORNs, but synaptic reliability is also important because it should help ensure that

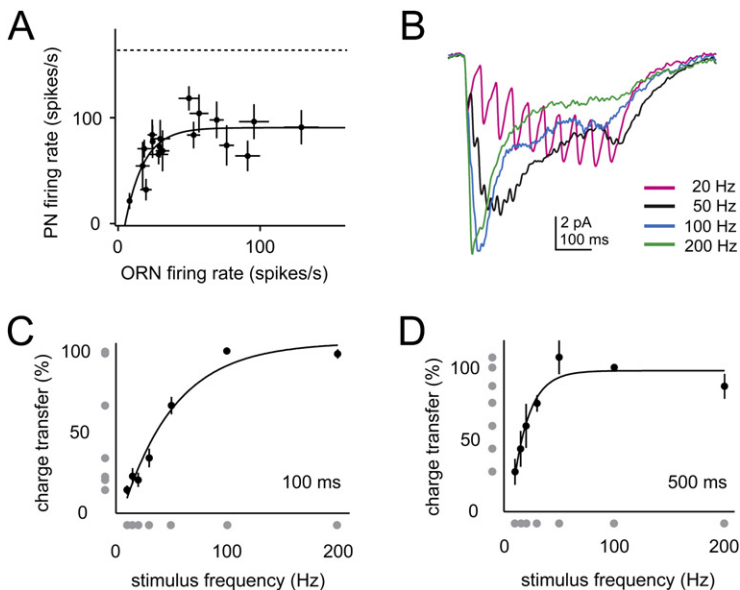


Figure 9. Synaptic Depression Produces a Nonlinear Relationship between Presynaptic Firing Rate and Post-synaptic Current

(A) The relationship between ORN and PN odor responses is non-linear. Each point represents a different odor, and the frequency of PN spikes evoked by that odor is plotted versus the frequency of ORN spikes evoked by the same odor. All ORNs and PNs correspond to glomerulus VM2. Each point represents the average of at least four experiments in different flies. Frequency is calculated over a 500 ms period of odor stimulation. Line is an exponential fit. Panel reproduced from Bhandawat et al. (2007). Dotted line indicates the average maximum frequency at which PNs can fire constantly over a 500 ms period of somatic current injection (n = 8 cells). (B) Synaptic current recorded in PNs in response to trains of antennal nerve stimulation at various frequencies. Every experiment was preceded by antennal nerve stimulation mimicking spontaneous ORN firing rates (7 Hz, 4 s). Each trace is an average of several sweeps per cell, averaged across four cells. All recordings in (B)–(D) are from PNs in glomerulus VM2.

(C and D) Total charge transfer during the first 100 ms (C) or 500 ms (D) of antennal nerve stimulation, plotted against stimulus frequency (normalized to the value at 100 Hz). Each point represents mean \pm SEM averaged across experiments (n = 4). Lines are exponential fits. Gray points are projections of the data points onto the x and y axes showing the distribution of stimulus frequency and charge transfer, respectively. Note that points that are clustered together on the x axis become more uniformly separated on the y axis (see Discussion).

only minimal noise is added in the PN layer, allowing PN reliability to approach the theoretical limit dictated by the ORN-PN convergence ratio and the amount of noise in the ORN layer.

Size Matching

Large cells generally have lower input resistances than small cells, so it is more difficult to depolarize large cells to the threshold of spike initiation. This has long been recognized as an interesting problem in neuromuscular physiology. Fatt and Katz (1952) noticed that a quantum of neurotransmitter produces a smaller depolarization in a large muscle cell in the thigh as compared with a small muscle cell in the toe. Subsequently, Katz and Thesleff (1957) recognized that this is due to the lower input resistance of the larger muscle cell. To compensate, motoneurons synapsing onto large muscle cells generally form large axonal arbors containing many vesicular release sites. This ensures that a single motoneuron spike can trigger muscle contraction in both large and small muscles (Sanes and Lichtman, 1999; Wood and Slater, 2001). A similar phenomenon occurs at the *Drosophila* neuromuscular junction (Lnenicka and Keshishian, 2000; Nakayama et al., 2006).

At the neuromuscular junction, this “size matching” phenomenon occurs not just across synapses but also within a synapse across time. During normal development, each muscle grows in size and its input resistance drops. This is matched by an increased quantal content, and sometimes also an increased quantal size (DeRosa and Govind, 1978; Lnenicka and Mellon, 1983; Pulver et al., 2005; Schuster et al., 1996).

Although size matching is well-established at the neuromuscular junction, it is almost unknown at synapses in the central nervous system. One study has described size matching during developmental growth at a single identified synapse in the mollusk central nervous system (Pawson and Chase, 1988),

but size matching across different central synapses has not been reported previously. Here we have shown that in the *Drosophila* antennal lobe, unitary synaptic potentials are uniform across PNs with variously sized dendritic tufts. Meanwhile, unitary synaptic currents are large in large glomeruli, and small in small glomeruli. We hypothesize that this represents a compensation for lower input resistance in large dendritic arbors. It should be noted that we cannot measure the input resistance of the dendritic compartment in PNs, so we cannot directly test this aspect of our hypothesis. Furthermore, we do not know how the signals we are monitoring correspond to signals at the spike initiation zone.

If a large dendritic arbor makes it harder for a cell to reach threshold, why do some PNs have large dendritic arbors? In the neuromuscular system, the diversity in postsynaptic size has an obvious physiological function: thigh muscle fibers are necessarily larger than toe muscle fibers. In the *Drosophila* olfactory system, it turns out that the volume occupied by a particular PN’s dendritic arbor is correlated with the number of ORN axons innervating that volume. We measured the size of 12 identified glomeruli and found a strong linear correlation between glomerular volume and the number of ORNs presynaptic to each glomerulus (Figure S7; ORN data are from de Bruyne et al., 1999, 2001; Shanbhag et al., 1999). Thus, a PN with a large dendritic arbor pools inputs from many presynaptic axons. We propose that the magnitudes of postsynaptic currents are adjusted to ensure that the postsynaptic impact of a single spike is the same whether PNs have large or small dendritic arbors. If so, the net result would be a higher sensitivity of PNs in larger glomeruli. This idea is consistent with the observation that some of the largest glomeruli are related to pheromone perception (Kurtovic et al., 2007; Schlieff and Wilson, 2007; van der Goes van Naters and Carlson, 2007).

Homeostatic Control of Synaptic Efficacy

We propose that size matching in antennal lobe PNs represents a homeostatic phenomenon—that is, the outcome of a process whereby some output variable (here, uEPSP amplitude) is precisely maintained at a constant level via a feedback mechanism (Davis, 2006). In support of this hypothesis, we found that a genetic manipulation that decreases the input resistance of a PN produced an increased uEPSC amplitude in that cell. This is direct evidence that unitary synaptic currents are scaled to match to the intrinsic properties of PNs. This also supports the idea that PNs with large dendritic arbors have stronger synapses because these dendrites are harder to depolarize.

Many studies have demonstrated that specific aspects of neural activity are under homeostatic control (reviewed in Davis, 2006; Marder and Goaillard, 2006; Perez-Otano and Ehlers, 2005; Turrigiano, 2007). Interestingly, homeostatic set points are not necessarily defined by total postsynaptic activity. During development, some cells can maintain tight homeostatic regulation of uEPSPs while permitting changes in total activity (Pulver et al., 2005). Similar to this, we have found that PNs of different sizes have matched uEPSPs, but nevertheless these PNs show very different levels of total spontaneous activity (R.I.W., unpublished data), due to the different numbers of ORNs presynaptic to each glomerulus and the different spontaneous firing rates of these ORN types. If size matching in PNs does reflect homeostatic regulation, then the set point for this system must be defined in terms of uEPSPs, not total postsynaptic spike rates. This is consistent with the general observation that some parameters of cellular or network activity can be under homeostatic control while other parameters float freely (Bucher et al., 2005; Davis, 2006). For example, the *Drosophila* neuromuscular junction can compensate for a small change in the amount of depolarization produced by individual synaptic vesicles, but is insensitive to the overall level of activity at the synapse (Frank et al., 2006).

Implications of Short-Term Synaptic Depression for Neural Coding

Our results show that the probability of release p is uniformly high across glomeruli. High p tends to promote synaptic depression at high stimulus frequencies (Zucker and Regehr, 2002), and indeed we observe strong short-term depression at these synapses. Many mechanisms in addition to vesicular depletion are likely to contribute to this depression (presynaptic inhibition, for example). We observed strong depression at all frequencies above about 50 spikes/s. Since odors can easily trigger sustained ORN firing rates well above 200 spikes/s (de Bruyne et al., 1999, 2001; Hallem and Carlson, 2006), short-term depression is likely to occur during natural olfactory experience.

Synaptic depression is probably a major reason why PN odor responses are more transient than the responses of the presynaptic ORNs (Bhandawat et al., 2007). This transience should emphasize the onset of odor stimuli. It should also promote adaptation to persistently strong odor stimuli.

Synaptic depression is also likely to be a major reason why PNs are more broadly tuned to odors than their presynaptic ORNs (Bhandawat et al., 2007; Wilson et al., 2004). Because ORN-PN synapses depress rapidly at high spike rates, strong,

sustained ORN responses will not be transmitted as effectively as weak, sustained ORN responses. This will tend to broaden steady-state odor tuning in PNs. From a theoretical point of view, it has been noted that synaptic depression should broaden the tuning of postsynaptic cells (Abbott et al., 1997). Here we have shown that strong synaptic depression actually occurs at a synapse where there is clear evidence in vivo that postsynaptic neurons are more broadly tuned to stimuli than presynaptic neurons are.

Broad PN tuning might be useful because it increases the separation between odor representations in PN coding space (Bhandawat et al., 2007). When a neuron uses its dynamic range efficiently in this way, sensory representations are better protected from contamination by noise added at later processing stages (Laughlin, 1981; Laughlin et al., 1987). This idea is illustrated by the gray symbols in Figure 9C and especially Figure 9D: note that responses are more evenly distributed on the y axis compared with the x axis. In these experiments, we stimulated ORN axons with a distribution of frequencies mimicking the distribution of odor-evoked ORN in vivo firing rates described in previous studies (Bhandawat et al., 2007; de Bruyne et al., 2001; Hallem and Carlson, 2006). We used mainly low stimulus frequencies (mimicking the weak responses that are commonly observed in these neurons) and just a few high stimulus frequencies (mimicking sparse, strong ORN odor responses). Overall, the tuning of our stimulus distribution was similar to the odor tuning of a typical ORN (Bhandawat et al., 2007; de Bruyne et al., 2001; Hallem and Carlson, 2006). Because of synaptic depression, synaptic charge in PNs was more broadly tuned than the original distribution of presynaptic stimulus frequencies (Figures 9C and 9D).

It should be noted that other mechanisms likely also broaden PN tuning. PNs receive lateral excitatory inputs from other glomeruli (Olsen et al., 2007; Root et al., 2007; Shang et al., 2007). Because the odor tuning of lateral input to a PN differs from the odor tuning of direct ORN input (Olsen et al., 2007), these lateral excitatory connections should decrease the odor selectivity of PNs. Intrinsic properties of PNs may also play a role. Although PNs are capable of firing at very high rates, firing rates only grow sublinearly with increasing synaptic currents (data not shown), due to the relative refractory period.

In sum, we suggest that primary olfactory synapses in *Drosophila* are optimized for high sensitivity near odor detection thresholds. When ORN firing rates are low, ORN-PN synapses are very strong. These synapses have a high and consistent quantal content at low presynaptic firing rates, and this should improve detection sensitivity by minimizing synaptic noise. Additionally, because PNs receive strong synapses from ORNs in both antennae, each PN pools signals from many presynaptic inputs, which should further improve response reliability and increase sensitivity. Large PNs with low input resistance can maintain this high sensitivity because synaptic currents are particularly large in these cells. Taken together, these mechanisms should produce high sensitivity to weak odors. Behavioral odor detection thresholds in *Drosophila* have not been measured in detail, but experiments in moths suggest that thresholds can be extremely low (Rau and Rau, 1929; Schneider et al., 1968).

When odor stimuli are much stronger than threshold concentrations, synaptic depression causes PN responses to be transient. This should promote perceptual adaptation to lingering odors. Synaptic depression also makes PNs less sensitive to strong ORN signals as compared with weak ORN signals. This should promote the discriminability of odor stimuli that activate the ORN ensemble weakly, at the expense of strong and less ambiguous stimuli. If genetic manipulations can be used to selectively alter the properties of ORN-PN synapses, then it should be possible in the future to put some of these ideas to the test.

EXPERIMENTAL PROCEDURES

Fly Stocks

Flies were raised on conventional cornmeal agar under a 12 hr light/12 hr dark cycle at 25°C, except for *NP3062-Gal4,UAS-CD8:GFP/+;UAS-Kir2.1^{AAE}-GFP/+* flies, which were raised at 29°C to increase the efficacy of the Gal4/UAS expression system. All experiments were performed on adult female flies, 2–7 days posteclosion. Stocks were kindly provided as follows: *NP3062-Gal4*, *NP5103-Gal4*, and *NP7217-Gal4* (Kei Ito and Liqun Luo); *GH146-Gal4* (Liqun Luo); *UAS-Kir2.1^{AAE}-GFP* and *UAS-Kir2.1-GFP* (Graeme Davis). *UAS-CD8:GFP (X)* and *UAS-CD8:GFP (II)* lines were obtained from the Bloomington stock center.

PN Recordings

Whole-cell patch-clamp recordings from PNs were performed as previously described (Wilson and Laurent, 2005; Wilson et al., 2004). The internal patch-pipette solution used for voltage-clamp recordings contained the following: 140 mM cesium aspartate, 10 mM HEPES, 4 mM MgATP, 0.5 mM Na₃GTP, 1 mM EGTA, 1 mM KCl, 13 mM biocytin hydrazide, and 10 mM QX-314 (pH = 7.3, osmolarity adjusted to ~265 mOsm). For current-clamp experiments, QX-314 was removed and cesium was replaced with an equal concentration of potassium. External saline contained 103 mM NaCl, 3 mM KCl, 5 mM *N*-tris(hydroxymethyl) methyl-2-aminoethane-sulfonic acid, 8 mM trehalose, 10 mM glucose, 26 mM NaHCO₃, 1 mM NaH₂PO₄, 1.5 mM CaCl₂, and 4 mM MgCl₂ (osmolarity adjusted to 270–275 mOsm). The saline was bubbled with 95% O₂/5% CO₂ and reached a pH of 7.3. Recordings were acquired with an Axopatch 200A amplifier (Axon Instruments) equipped with a CV 201A headstage (500 M Ω). In voltage-clamp recordings, the command potential was –65 mV. Signals were low-pass filtered at 1 kHz and digitized at 5 kHz. Voltages are uncorrected for liquid junction potential. The following strains were used to record from specific types of PNs: *NP3062-Gal4,UAS-CD8:GFP* (DM6, DL5, and DM4 PNs), *NP5103-Gal4,UAS-CD8:GFP* (VM2 PNs), and *NP7217-Gal4,UAS-CD8:GFP* (DM6, VM2, DL5, and VM7 PNs). In experiments where the PN type is not reported, recordings were from the genotype *GH146-Gal4,UAS-CD8:GFP* (Figures 1B and 1C and Figure 2B). One neuron was recorded per brain, and the morphology of each cell was visualized post hoc with biocytin immunohistochemistry. Immunohistochemistry with biocytin-streptavidin, rat anti-CD8, and mouse nc82 antibody was performed as described previously (Wilson and Laurent, 2005), except that in the secondary incubation we used 1:250 goat anti-mouse: Alexa Fluor 633 and 1:1000 streptavidin: Alexa Fluor 568 (Molecular Probes). The nc82 antibody used to outline glomerular boundaries was obtained from the Developmental Studies Hybridoma Bank (U. of Iowa).

Stimulation of ORN Axons

Immediately prior to recording, fine forceps were used to gently sever the antennal nerves at their point of entry into the first antennal segment. Care was taken not to pull the nerve along its long axis and damage the axons during the operation. To stimulate ORN axons, part of the antennal nerve was drawn into a saline-filled suction electrode and a brief pulse (50 μ s) of current was passed through the nerve using a stimulus isolator (AMPI, Jerusalem, Israel). At the end of some experiments, 50 μ M mecamylamine (Sigma) was added to the saline to verify that evoked EPSCs are mediated by nicotinic acetylcho-

line receptors. Except for the recordings in Figure 1, a minimal stimulation protocol was used throughout the study to stimulate only one ORN axon that was directly presynaptic to the recorded PN (Allen and Stevens, 1994; Dobrunz and Stevens, 1997; Raastad et al., 1992; Stevens and Wang, 1995). See Supplemental Experimental Procedures for details on the criteria for minimal stimulation and stimulus stability. After collecting uEPSCs, 1 μ M tetrodotoxin was added to the external saline and mEPSCs were recorded in the same cell for 20 min. For multiple-probability fluctuation analysis (Clements, 2003; Clements and Silver, 2000; Silver, 2003), ~25 uEPSCs were collected under each condition with a different probability of vesicular release. The probability of release was modified by adding various amounts of Cd²⁺ to the external saline. To record purely lateral synaptic excitation to a PN, both the antennae and palps were removed with fine forceps immediately prior to recording. One antennal nerve was stimulated with a suction electrode while recording from a VM7 palp PN. To assess the contribution of lateral (slow) synaptic excitation to our measurement of the amplitude of direct (fast) EPSCs, we measured the amplitude of lateral EPSCs at the time point when direct EPSCs peak (see also Figure S6). The stimulus artifact is shown in all traces but is clipped for clarity in some cases.

Kir2.1 Overexpression

Kir2.1 potassium channel was overexpressed in a specific subset of PNs to decrease their input resistance. Because the *NP3062-Gal4* line drives Gal4 expression in exactly one PN postsynaptic to DM4 and one PN postsynaptic to DL5 (plus a few VM2 and DM6 PNs), any effects of this manipulation should be cell autonomous in glomeruli DM4 and DL5. We overexpressed the form of Kir2.1 that lacks a functional PDZ-interacting sequence (Kir2.1^{AAE}) in order to avoid displacing other PDZ-interacting proteins from the postsynaptic density (Paradis et al., 2001). Input resistance values (Figure 4D) were obtained just after breaking into the cell. We observed that just after break-in, input resistance did not depend on the composition of the internal patch-pipette solution ($p > 0.52$, *t* test, Cs⁺ versus K⁺, *n* = 9 versus 5), meaning that Cs⁺ does not diffuse immediately throughout the cell. For Figures 4D and 4E, we used a Cs⁺-based pipette internal to maintain consistency with other voltage-clamp experiments in this study. When Cs⁺ was included in the internal patch-pipette solution, input resistance in Kir2.1-overexpressing PNs increased to control levels over time. This is evidence that the decrease in input resistance was specifically caused by overexpression of Kir2.1. This also implies that input resistance measured at the soma reflects the input resistance of nonsomatic compartments to some extent. Kir2.1 overexpression did not affect the morphology of these PNs.

Data Analysis

Unless stated otherwise, all analyses were performed in Igor Pro (Wavemetrics) using custom software. All mean values are reported as mean \pm SEM, averaged across experiments. See Supplemental Experimental Procedures for details on multiple-probability fluctuation analysis, measurement of mEPSCs, estimation of *N* and *p* at a single release probability, analysis of trains (Figure 8G), and image analysis.

SUPPLEMENTAL DATA

The Supplemental Data for this article can be found online at <http://www.neuron.org/cgi/content/full/58/3/401/DC1>.

ACKNOWLEDGMENTS

We thank Kei Ito, Liqun Luo, Christopher Potter, and Graeme Davis for gifts of fly stocks, and Bruce Bean for the loan of equipment. We are grateful to Thomas Schwarz, Gregory Jefferis, Bernardo Sabatini, and members of the Wilson Lab for helpful conversations and comments on the manuscript. This work was funded by a grant from the NIH (1R01DC008174-01), a Pew Scholar Award, a McKnight Scholar Award, a Sloan Foundation Research Fellowship, and a Beckman Young Investigator Award (to R.I.W.). H.K. was partially supported by a Postdoctoral Fellowship from the Uehara Memorial Foundation.

Received: October 3, 2007
Revised: January 30, 2008
Accepted: February 25, 2008
Published: May 7, 2008

REFERENCES

- Abbott, L.F., Varela, J.A., Sen, K., and Nelson, S.B. (1997). Synaptic depression and cortical gain control. *Science* 275, 220–224.
- Allen, C., and Stevens, C.F. (1994). An evaluation of causes for unreliability of synaptic transmission. *Proc. Natl. Acad. Sci. USA* 91, 10380–10383.
- Bargmann, C.I. (2006). Comparative chemosensation from receptors to ecology. *Nature* 444, 295–301.
- Bhandawat, V., Olsen, S.R., Schlieff, M.L., Gouwens, N.W., and Wilson, R.I. (2007). Sensory processing in the *Drosophila* antennal lobe increases the reliability and separability of ensemble odor representations. *Nat. Neurosci.* 10, 1474–1482.
- Biro, A.A., Holderith, N.B., and Nusser, Z. (2005). Quantal size is independent of the release probability at hippocampal excitatory synapses. *J. Neurosci.* 25, 223–232.
- Bucher, D., Prinz, A.A., and Marder, E. (2005). Animal-to-animal variability in motor pattern production in adults and during growth. *J. Neurosci.* 25, 1611–1619.
- Christie, J.M., and Jahr, C.E. (2006). Multivesicular release at Schaffer collateral-CA1 hippocampal synapses. *J. Neurosci.* 26, 210–216.
- Clements, J.D. (2003). Variance-mean analysis: a simple and reliable approach for investigating synaptic transmission and modulation. *J. Neurosci. Methods* 130, 115–125.
- Clements, J.D., and Silver, R.A. (2000). Unveiling synaptic plasticity: a new graphical and analytical approach. *Trends Neurosci.* 23, 105–113.
- Comer, C.M., and Robertson, R.M. (2001). Identified nerve cells and insect behavior. *Prog. Neurobiol.* 63, 409–439.
- Couto, A., Alenius, M., and Dickson, B.J. (2005). Molecular, anatomical, and functional organization of the *Drosophila* olfactory system. *Curr. Biol.* 15, 1535–1547.
- Davis, G.W. (2006). Homeostatic control of neural activity: from phenomenology to molecular design. *Annu. Rev. Neurosci.* 29, 307–323.
- de Bruyne, M., Clyne, P.J., and Carlson, J.R. (1999). Odor coding in a model olfactory organ: the *Drosophila* maxillary palp. *J. Neurosci.* 19, 4520–4532.
- de Bruyne, M., Foster, K., and Carlson, J.R. (2001). Odor coding in the *Drosophila* antenna. *Neuron* 30, 537–552.
- DeRosa, R.A., and Govind, C.K. (1978). Transmitter output increases in an identifiable lobster motoneurone with growth of its muscle fibres. *Nature* 273, 676–678.
- Dobrunz, L.E., and Stevens, C.F. (1997). Heterogeneity of release probability, facilitation, and depletion at central synapses. *Neuron* 18, 995–1008.
- Elmore, T., Ignell, R., Carlson, J.R., and Smith, D.P. (2003). Targeted mutation of a *Drosophila* odor receptor defines receptor requirement in a novel class of sensillum. *J. Neurosci.* 23, 9906–9912.
- Faber, D.S., and Korn, H. (1991). Applicability of the coefficient of variation method for analyzing synaptic plasticity. *Biophys. J.* 60, 1288–1294.
- Fatt, P., and Katz, B. (1952). Spontaneous subthreshold activity at motor nerve endings. *J. Physiol.* 117, 109–128.
- Fishilevich, E., and Vosshall, L.B. (2005). Genetic and functional subdivision of the *Drosophila* antennal lobe. *Curr. Biol.* 15, 1548–1553.
- Frank, C.A., Kennedy, M.J., Goold, C.P., Marek, K.W., and Davis, G.W. (2006). Mechanisms underlying the rapid induction and sustained expression of synaptic homeostasis. *Neuron* 52, 663–677.
- Hallem, E.A., and Carlson, J.R. (2004). The odor coding system of *Drosophila*. *Trends Genet.* 20, 453–459.
- Hallem, E.A., and Carlson, J.R. (2006). Coding of odors by a receptor repertoire. *Cell* 125, 143–160.
- Hallem, E.A., Ho, M.G., and Carlson, J.R. (2004). The molecular basis of odor coding in the *Drosophila* antenna. *Cell* 117, 965–979.
- Katz, B. (1969). *The Release of Neural Transmitter Substances* (Liverpool, UK: Liverpool University Press).
- Katz, B., and Thesleff, S. (1957). On the factors which determine the amplitude of the miniature end-plate potential. *J. Physiol.* 137, 267–278.
- Kurtovic, A., Widmer, A., and Dickson, B.J. (2007). A single class of olfactory neurons mediates behavioural responses to a *Drosophila* sex pheromone. *Nature* 446, 542–546.
- Laissue, P.P., Reiter, C., Hiesinger, P.R., Halter, S., Fischbach, K.F., and Stocker, R.F. (1999). Three-dimensional reconstruction of the antennal lobe in *Drosophila melanogaster*. *J. Comp. Neurol.* 405, 543–552.
- Laughlin, S. (1981). A simple coding procedure enhances a neuron's information capacity. *Z. Naturforsch. [C]* 36, 910–912.
- Laughlin, S.B., Howard, J., and Blakeslee, B. (1987). Synaptic limitations to contrast coding in the retina of the blowfly *Calliphora*. *Proc. R. Soc. Lond. B. Biol. Sci.* 237, 437–467.
- Laurent, G., and Hustert, R. (1988). Motor neuronal receptive fields delimit patterns of motor activity during locomotion of the locust. *J. Neurosci.* 8, 4349–4366.
- Lnenicka, G.A., and Mellon, D., Jr. (1983). Changes in electrical properties and quantal current during growth of identified muscle fibres in the crayfish. *J. Physiol.* 345, 261–284.
- Lnenicka, G.A., and Keshishian, H. (2000). Identified motor terminals in *Drosophila* larvae show distinct differences in morphology and physiology. *J. Neurobiol.* 43, 186–197.
- Marder, E., and Goaillard, J.M. (2006). Variability, compensation and homeostasis in neuron and network function. *Nat. Rev. Neurosci.* 7, 563–574.
- Meyer, A.C., Neher, E., and Schneggenburger, R. (2001). Estimation of quantal size and number of functional active zones at the calyx of held synapse by nonstationary EPSC variance analysis. *J. Neurosci.* 21, 7889–7900.
- Milo, R., Shen-Orr, S., Itzkovitz, S., Kashtan, N., Chklovskii, D., and Alon, U. (2002). Network motifs: simple building blocks of complex networks. *Science* 298, 824–827.
- Murphy, G.J., Glickfeld, L.L., Balsen, Z., and Isaacson, J.S. (2004). Sensory neuron signaling to the brain: properties of transmitter release from olfactory nerve terminals. *J. Neurosci.* 24, 3023–3030.
- Nakayama, H., Kazama, H., Nose, A., and Morimoto-Tanifuji, T. (2006). Activity-dependent regulation of synaptic size in *Drosophila* neuromuscular junctions. *J. Neurobiol.* 66, 929–939.
- Oertner, T.G., Sabatini, B.L., Nimchinsky, E.A., and Svoboda, K. (2002). Facilitation at single synapses probed with optical quantal analysis. *Nat. Neurosci.* 5, 657–664.
- Olsen, S.R., Bhandawat, V., and Wilson, R.I. (2007). Excitatory interactions between olfactory processing channels in the *Drosophila* antennal lobe. *Neuron* 54, 89–103.
- Paradis, S., Sweeney, S.T., and Davis, G.W. (2001). Homeostatic control of presynaptic release is triggered by postsynaptic membrane depolarization. *Neuron* 30, 737–749.
- Pawson, P.A., and Chase, R. (1988). The development of transmission at an identified molluscan synapse. II. A quantal analysis of transmission. *J. Neurophysiol.* 60, 2211–2222.
- Perez-Otano, I., and Ehlers, M.D. (2005). Homeostatic plasticity and NMDA receptor trafficking. *Trends Neurosci.* 28, 229–238.
- Pouille, F., and Scanziani, M. (2001). Enforcement of temporal fidelity in pyramidal cells by somatic feed-forward inhibition. *Science* 293, 1159–1163.
- Pulver, S.R., Bucher, D., Simon, D.J., and Marder, E. (2005). Constant amplitude of postsynaptic responses for single presynaptic action potentials but not bursting input during growth of an identified neuromuscular junction in the lobster, *Homarus americanus*. *J. Neurobiol.* 62, 47–61.

- Raastad, M., Storm, J.F., and Andersen, P. (1992). Putative single quantum and single fibre excitatory postsynaptic currents show similar amplitude range and variability in rat hippocampal slices. *Eur. J. Neurosci.* *4*, 113–117.
- Rau, P., and Rau, N. (1929). The sex attraction and rhythmic periodicity in giant saturniid moths. *Trans. Acad. Sci. St Louis* *26*, 80–221.
- Root, C.M., Semmelhack, J.L., Wong, A.M., Flores, J., and Wang, J.W. (2007). Propagation of olfactory information in *Drosophila*. *Proc. Natl. Acad. Sci. USA* *104*, 11826–11831.
- Sanes, J.R., and Lichtman, J.W. (1999). Development of the vertebrate neuromuscular junction. *Annu. Rev. Neurosci.* *22*, 389–442.
- Sargent, P.B., Saviane, C., Nielsen, T.A., DiGregorio, D.A., and Silver, R.A. (2005). Rapid vesicular release, quantal variability, and spillover contribute to the precision and reliability of transmission at a glomerular synapse. *J. Neurosci.* *25*, 8173–8187.
- Schlieff, M.L., and Wilson, R.I. (2007). Olfactory processing and behavior downstream from highly selective receptor neurons. *Nat. Neurosci.* *10*, 623–630.
- Schneider, D., Kasang, G., and Kaissling, K.E. (1968). Bestimmung der riechschwelle von *Bombyx mori* mit tritium-markiertem bombykol. *Naturwissenschaften* *55*, 395.
- Schuster, C.M., Davis, G.W., Fetter, R.D., and Goodman, C.S. (1996). Genetic dissection of structural and functional components of synaptic plasticity. I. Fasciclin II controls synaptic stabilization and growth. *Neuron* *17*, 641–654.
- Shanbhag, S.R., Muller, B., and Steinbrecht, R.A. (1999). Atlas of olfactory organs of *Drosophila melanogaster*. 1. Types, external organization, innervation, and distribution of olfactory sensilla. *Int. J. Insect Morphol. Embryol.* *28*, 377–397.
- Shang, Y., Claridge-Chang, A., Sjulson, L., Pypaert, M., and Miesenböck, G. (2007). Excitatory local circuits and their implications for olfactory processing in the fly antennal lobe. *Cell* *128*, 601–612.
- Silver, R.A. (2003). Estimation of nonuniform quantal parameters with multiple-probability fluctuation analysis: theory, application and limitations. *J. Neurosci. Methods* *130*, 127–141.
- Silver, R.A., Lubke, J., Sakmann, B., and Feldmeyer, D. (2003). High-probability unquantal transmission at excitatory synapses in barrel cortex. *Science* *302*, 1981–1984.
- Stevens, C.F., and Wang, Y. (1995). Facilitation and depression at single central synapses. *Neuron* *14*, 795–802.
- Stocker, R.F., Lienhard, M.C., Borst, A., and Fischbach, K.F. (1990). Neuronal architecture of the antennal lobe in *Drosophila melanogaster*. *Cell Tissue Res.* *262*, 9–34.
- Strausfeld, N.J. (1976). *Atlas of an Insect Brain* (Berlin: Springer).
- Turrigiano, G. (2007). Homeostatic signaling: the positive side of negative feedback. *Curr. Opin. Neurobiol.* *17*, 318–324.
- van der Goes van Naters, W., and Carlson, J.R. (2007). Receptors and neurons for fly odors in *Drosophila*. *Curr. Biol.* *17*, 606–612.
- Walmsley, B., Alvarez, F.J., and Fyffe, R.E. (1998). Diversity of structure and function at mammalian central synapses. *Trends Neurosci.* *21*, 81–88.
- Wilson, R.I., and Laurent, G. (2005). Role of GABAergic inhibition in shaping odor-evoked spatiotemporal patterns in the *Drosophila* antennal lobe. *J. Neurosci.* *25*, 9069–9079.
- Wilson, R.I., and Mainen, Z.F. (2006). Early events in olfactory processing. *Annu. Rev. Neurosci.* *29*, 163–201.
- Wilson, R.I., Turner, G.C., and Laurent, G. (2004). Transformation of olfactory representations in the *Drosophila* antennal lobe. *Science* *303*, 366–370.
- Wood, S.J., and Slater, C.R. (2001). Safety factor at the neuromuscular junction. *Prog. Neurobiol.* *64*, 393–429.
- Zucker, R.S., and Regehr, W.G. (2002). Short-term synaptic plasticity. *Annu. Rev. Physiol.* *64*, 355–405.